Mono- and Binuclear Molybdenum and Tungsten Complexes Containing Asymmetric Bridging Ligands: Effects of Ligand Conjugation and Conformation on Metal–Metal Interactions

Amitava Das, John C. Jeffery, John P. Maher, Jon A. McCleverty,* Erik Schatz, Michael D. Ward,* and Gerd Wollermann

School of Chemistry, University of Bristol, Cantock's Close, Bristol BS8 1TS, U.K.

Received October 15, 1992

We have prepared the new monodentate ligands 4-(4-methoxyphenyl)pyridine, 1-(4-pyridyl)-2-(4-methoxyphenyl)-ethene, 1-(4-pyridyl)-2-(3-methoxyphenyl)ethene, and 1-(3-pyridyl)-2-(4-methoxyphenyl)ethene (L^5–L^8); demethylation of the methoxy group in each case afforded the new bridging bidentate ligands HL^1–HL^4, which contain one pyridyl and one phenolate donor. Attachment of a MoL*(NO)Cl [L* = hydrotris(3,5-dimethylpyrazolyl)-borate] moiety to the pyridyl groups of L^5–L^8 gave the 17-electron complexes [Mo(NO)L*ClL'] (L' = L^5–L^8, complexes **5–8**). Reaction of HL^1–HL^4 with [M(NO)L*Cl_2] (M = Mo, W) afforded the mononuclear 16-electron complexes [M(NO)L*ClL'] (M = Mo, L' = L^1–L^4, complexes **1–4**; M = W, L' = L^1–L^4, complexes **13–16**), in which the phenolate terminus of L^1–L^4 is attached to the metal and the pyridyl group is pendant in each case. The pyridyl groups were N-methylated with CH_3I to afford $[9]^+$–$[12]^+$ and $[17]^+$–$[20]^+$, respectively. Alternatively, a second MoL*(NO)Cl could be attached to the pendant pyridyl groups of **1–4** to give the binuclear complexes [Mo(NO)L*Cl(μ-L')Mo(NO)L*Cl] (L' = L^1–L^4, complexes **21–24**), which contain a 16-electron Mo center at the phenolate terminus and a 17-electron Mo center at the pyridyl terminus. Electrochemical studies showed that the anodic shift of the 16e–17e reduction due to N-methylation in $[9]^+$–$[12]^+$ and $[17]^+$–$[20]^+$ varies with the ligand in the order $L^1 > (L^2 \approx L^4) > L^3$. This is explained by the extent to which the relative substitution patterns of the component aromatic rings allow communication between the halves; the halves of L^3 appear to be electrochemically isolated, and this is supported by the electronic spectra. A similar pattern for the electrochemical interactions was observed in binuclear complexes **21–24**. EPR studies showed that in **21–24** the unpaired electron is localized at the pyridyl-substituted Mo center, which is expected considering the difference in redox potentials between the two ends. However on one-electron reduction of the 16-electron phenolate-substituted Mo center to give binuclear complexes with *two* 17-electron centers, the spectra indicate that the two electrons are in fast exchange on the EPR time scale with both electrons coupled to both nuclei. The crystal structure of **5** shows that the 4-(4-methoxyphenyl)-pyridine ligand is nearly planar, probably because charge transfer from the electron-donating methoxy group to the electron-accepting pyridyl group results in a quinonoidal contribution to the ligand structure.

Introduction

The study of binuclear metal complexes in which the metals are linked by an unsaturated bridging ligand is of particular interest with regard to the study of electron transfer in mixed-valence systems.[1] The archetypal example is the Creutz–Taube ion,[1b] the theoretical study of which has received a great deal of attention and thereby contributed considerably to our understanding of electron-transfer theory.[2] A particularly popular bridging ligand which has long been the focus of much attention is 4,4'-bipyridine, and many binuclear complexes containing 4,4'-bipyridine or a derivative as a bridging ligand have been prepared to enable examination of metal–metal interactions across the bridging ligand.[3] Studies have also been performed on "extended" analogues of 4,4'-bipyridine (the α,ω-dipyridylpolyenes) with up to five trans double bonds between two 4-pyridyl groups, in order to determine the effects of the length of the "molecular wire" on electron-transfer and metal–metal interactions.[4]

A recent report describes the preparation and properties of [{Mo(NO)L*Cl}$_2$(μ-4,4'-bipy)] [L* = hydrotris(3,5-dimethylpyrazolyl)borate], a symmetrical binuclear complex for which EPR spectroscopy showed fast exchange of the two unpaired electrons between the two 17-electron molybdenum centers and a separation of 765 mV between the two one-electron reductions.[5] In view of the unusual behavior of this complex, we have been studying metal–metal interactions and electron delocalization in *asymmetric* binuclear complexes in which the metal centers at each end of the bridging ligand have different donor sets and, therefore, redox potentials. In this paper we wish to report the preparation, electrochemical, and EPR and electronic spectroscopic properties of mono- and binuclear molybdenum and tungsten complexes based on the new ligands HL^1–HL^4 and L^5–L^8 (Figure 1). Part of this work was recently published as a preliminary communication.[6]

(1) (a) Hush, N. S. *Prog. Inorg. Chem.* **1967**, *8*, 391. (b) Robin, M. B.; Day, P. *Adv. Inorg. Chem. Radiochem.* **1967**, *10*, 247. (c) Creutz, C. *Prog. Inorg. Chem.* **1983**, *30*, 1. (d) Richardson, D. E.; Taube, H. *Coord. Chem. Rev.* **1984**, *60*, 107. (e) Lay, P. A.; Magnuson, R. H.; Taube, H. *Inorg. Chem.* **1988**, *27*, 2364. (f) Stebler, A.; Ammeter, J. H.; Furholz, U.; Ludi, A. *Inorg. Chem.* **1984**, *23*, 2764. (g) Geselowitz, D. A.; Kutner, W.; Meyer, T. J. *Inorg. Chem.* **1986**, *25*, 2015. (h) Ram, M. S.; Haim, A. *Inorg. Chem.* **1991**, *30*, 1319. (i) Hupp, J. T. *J. Am. Chem. Soc.* **1990**, *112*, 1563. (j) Clark, R. J. H.; Michael, D. J.; Yamashita, M. *J. Chem. Soc., Dalton Trans.* **1991**, 3447. (k) Kitagawa, H.; Kojima, N.; Sakai, H. *J. Chem. Soc., Dalton Trans.* **1991**, 3211.

(2) See refs 3–30 in: Cooper, B. J.; Vess, T. M.; Kalsbeck, W. A.; Wertz, D. W. *Inorg. Chem.* **1991**, *30*, 2286.

(3) (a) Powers, M. J.; Callahan, R. W.; Salmon, D. J.; Meyer, T. J. *Inorg. Chem.* **1976**, *15*, 894. (b) Sutton, J. E.; Taube, H. *Inorg. Chem.* **1981**, *20*, 3125. (c) Neyhart, G. A.; Meyer, T. J. *Inorg. Chem.* **1986**, *25*, 4807. (d) Blackbourn, R. L.; Hupp, J. T. *J. Phys. Chem.* **1988**, *92*, 2817. (e) Hanack, M.; Deger, S.; Lange, A. *Coord. Chem. Rev.* **1988**, *83*, 115. (f) Zulu, M. M.; Lees, A. J. *Inorg. Chem.* **1988**, *27*, 1139. (g) Zulu, M. M.; Lees, A. J. *Inorg. Chem.* **1989**, *28*, 85. (h) Loeb, B. L.; Neyhart, G. A.; Worl, L. A.; Danielsen, E.; Sullivan, B. P.; Meyer, T. J. *J. Phys. Chem.* **1989**, *93*, 717. (i) Constable, E. C.; Ward, M. D. *J. Chem. Soc., Dalton Trans.* **1990**, 1405. (j) Downard, A. J.; Honey, G. E.; Phillips, L. F.; Steel, P. J. *Inorg. Chem.* **1991**, *30*, 2260. (k) Launay, J.-P.; Tourrel-Pagis, M.; Lipskier, J.-F.; Marvaud, V.; Joachim, C. *Inorg. Chem.* **1991**, *30*, 1033.

(4) (a) Woitellier, S.; Launay, J.-P.; Spangler, C. W. *Inorg. Chem.* **1989**, *28*, 758. (b) Thomas, J. A.; Jones, C. J.; McCleverty, J. A.; Collison, D.; Mabbs, F. E.; Harding, C. J.; Hutchings, M. G. *J. Chem. Soc., Chem. Commun.* **1992**, 1796.

(5) McWhinnie, S. L. W.; Jones, C. J.; McCleverty, J. A.; Collison, D.; Mabbs, F. E. *J. Chem. Soc., Chem. Commun.* **1990**, 940.

0020-1669/93/1332-2145$04.00/0

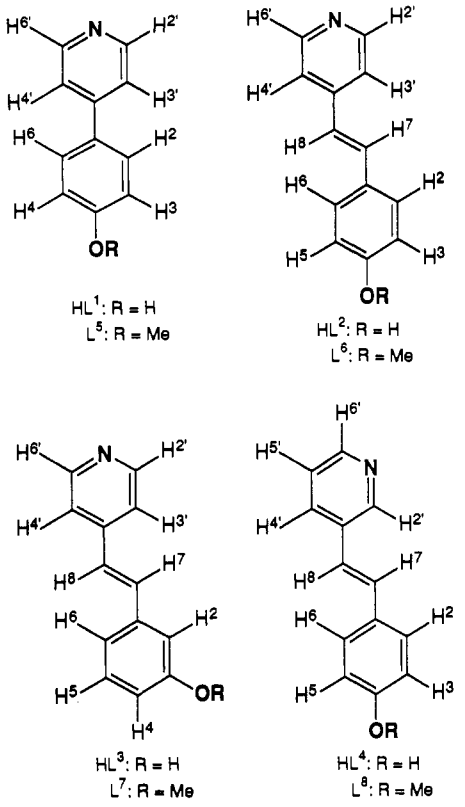

Figure 1. Structures of the new ligands, showing the numbering scheme used for the NMR data in Table I.

Experimental Section

General Details. ^{1}H NMR spectra were recorded on JEOL GX270 or GX400 spectrometers. Electron-impact (EI) mass spectra were obtained on a Kratos MS9 instrument, and fast-atom bombardment (FAB) mass spectra on a VG-Autospec instrument at the SERC Mass Spectrometry Service Centre, Swansea, U.K. EPR spectra were recorded on a Bruker ESP-300E spectrometer either at room temperature or at 77 K using a Dewar insert in the sample chamber. Reductions in situ with cobaltocene were performed simply by adding excess cobaltocene to the sample in an EPR tube at room temperature; the paramagnetic species thus produced were stable for several hours in the sealed EPR tube even in the presence of air. IR spectra were recorded in CH_2Cl_2 solution on a Perkin-Elmer 1600 Fourier-transform spectrometer, and electronic spectra on a Perkin-Elmer Lambda 2 spectrophotometer with distilled CH_2Cl_2 as solvent. Electrochemical experiments were performed using an EG&G PAR Model 273A potentiostat. A standard three-electrode configuration was used, with platinum-bead working and auxiliary electrodes and a saturated calomel electrode (SCE) reference. Ferrocene was added at the end of each experiment as an internal standard; all potentials are quoted vs the ferrocene/ferrocenium couple (Fc/Fc^+). The solvent was dichloromethane, purified by distillation from CaH_2, containing 0.1 mol dm^{-3} $[NBu_4][PF_6]$. Low-temperature chromatography was carried out with jacketed columns using a Haake KT 85 circulating cryostat. All reaction solvents were dried by standard methods before use. 4-Bromopyridine hydrochloride, 4-bromoanisole, methyl iodide, methyl chloroformate, *n*-butyllithium, diisopropylamine, 3-methoxybenzaldehyde, 4-methoxybenzaldehyde, 3-picoline, 4-picoline, and phosphoryl chloride were obtained from Aldrich. The picolines and diisopropylamine were distilled from CaH_2 immediately before use; all other reagents were used as received. Lithium diisopropylamide (LDA) was prepared immediately before use from equivalent amounts of *n*-butyllithium and diisopropylamine in hexane. The complexes $[Ni(PPh_3)_2Cl_2]$,[7] $[MoL^*(NO)Cl_2]$,[8] and $[WL^*(NO)Cl_2]$[8] were prepared according to published methods.

Preparation of 4-(4-Methoxyphenyl)pyridine (L^5). Method A. To an ice-cold, stirred suspension of anhydrous CuI (0.10 g, 0.53 mmol) and dry pyridine (1.19 g, 15 mmol) in dry tetrahydrofuran (thf, 25 cm^3) under N_2 was added methyl chloroformate (0.95 g, 10 mmol); a white precipitate appeared. The mixture was cooled to −30 °C, and a solution of the Grignard reagent prepared from 4-bromoanisole (2.06 g, 11 mmol) and Mg turnings (0.34 g, 14 mmol) in thf (20 cm^3) was added dropwise over 15 min. Stirring was continued for 15 min at −30 °C and then at room temperature for 1 h. After hydrolysis with aqueous NH_4Cl, thf was removed *in vacuo*, and the intermediate dihydropyridine was extracted with several portions of ether. The yellow extract was dried ($MgSO_4$) and evaporated to dryness to give a yellow oil. The oil was redissolved in acetone (20 cm^3) and rearomatized by dropwise addition of a solution of $KMnO_4$ in acetone at 0 °C until the purple color persisted. MnO_2 was removed by filtration through Celite. Removal of acetone left a yellow-brown solid, which was purified by chromatography on alumina (Aldrich, Brockmann activity I) with CH_2Cl_2 to yield 4-(4-methoxyphenyl)pyridine as a white solid (1.11 g, 60%). Mp: 95–96 °C (lit.[9] 95 °C).

Method B. To a stirred mixture of 4-bromopyridine (7.34 g, 46 mmol, freshly prepared by basification of an aqueous solution of the hydrochloride salt and extraction with ether followed by evaporation in vacuo at 0 °C) and $[Ni(PPh_3)_2Cl_2]$ (0.4 g, 0.6 mmol) in thf (70 cm^3) under N_2 at −10 °C (internal temperature) was added by cannula over 10 min a solution of the Grignard reagent prepared from 4-bromoanisole (11.2 g, 60 mmol) and Mg turnings (1.46 g, 60 mmol) in thf (50 cm^3). The internal temperature of the mixture was monitored carefully; after a few minutes it began to rise rapidly, and when it reached 40 °C, vigorous cooling was applied with a dry ice/acetone bath until the internal temperature dropped to 20 °C. This was repeated until no further spontaneous heating occurred, and the mixture was then left to stir at room temperature for a further 1 h. Dilute HCl (50 cm^3 of a 2 M solution) was added to quench the reaction, and most of the thf was removed *in vacuo*. The acidic solution was filtered, washed with ether (2 × 20 cm^3) to remove surplus bromoanisole and other organic impurities, and made basic with K_2CO_3 (use of KOH results in the coprecipitation of insoluble magnesium hydroxide which considerably complicates the subsequent extraction). The oil which separated was extracted with several portions of ether, and the combined extracts were dried ($MgSO_4$) and evaporated to give a crude yellow solid. Purification was either as in method A or by chromatography on SiO_2 with CH_2Cl_2 (95%)/CH_3OH (5%) to give 4-(4-methoxyphenyl)pyridine (6.4 g, 74%).

Preparation of L^6, L^7, and L^8. All three O-methylated ligands L^6–L^8 were prepared in the same way. The description given here for the preparation of L^6 is typical. To a solution of 4-picoline (1.86 g, 20 mmol) in tetrahydrofuran (thf, 10 cm^3) at 0 °C under N_2 was added dropwise a solution of LDA (20 mmol) in thf (10 cm^3). The pale yellow solution was then stirred for 1 h at 0 °C, after which time a solution of 4-methoxybenzaldehyde (2.72 g, 20 mmol) in thf (10 cm^3) was added dropwise with rapid stirring. The mixture was allowed to warm to room temperature and stirred overnight. After the reaction was quenched with water (5 cm^3), the mixture was evaporated to dryness. Extraction of the resulting solid with thf (50 cm^3) followed by evaporation yielded 1.58 g of the crude intermediate alcohol, which was dehydrated as follows without further purification.

The crude solid (1.58 g) was dissolved in dry pyridine (25 cm^3), and phosphoryl chloride (1.53 g, 10 mmol) was then added dropwise under N_2 with stirring. The mixture was stirred at room temperature for a further 1.5 h. Ice was added and the mixture left for 1 h to ensure complete destruction of residual $POCl_3$; the mixture was then evaporated to dryness. Water was added to the mixture, and concentrated HCl was added dropwise until all of the solid dissolved. After this acidic solution was washed with CH_2Cl_2 to remove organic impurities, the solution was made basic with NaOH and the resulting precipitate was collected by filtration, washed (H_2O), and dried. After recrystallization from aqueous methanol or chromatographic purification on Al_2O_3 with a mixture of CH_2Cl_2 (95%)/CH_3OH (5%), *trans*-1-(4-methoxyphenyl)-2-(4-pyridyl)-ethene (L^6) was isolated as a white powder (1.16 g, 28%).

Preparation of HL^1–HL^4. These were prepared by demethylation of L^5–L^8, respectively, with pyridinium chloride at 200 °C for 3 h according to a published procedure.[10] After the reaction mixture was cooled and water added, organic impurities were extracted with CH_2Cl_2 and the pH of the solution was then adjusted to approximately 6 with NaOH. The resulting precipitates were collected by filtration and recrystallized from

(6) Das, A.; Jeffery, J. C.; Maher, J. P.; McCleverty, J. A.; Schatz, E.; Ward, M. D.; Wollermann, G. *Angew. Chem., Int. Ed. Engl.* **1992**, *31*, 1515.
(7) Venanzi, L. M. *J. Chem. Soc.* **1958**, 719.
(8) (a) Jones, C. J.; McCleverty, J. A.; Reynolds, S. J.; Smith, C. F. *Inorg. Synth.* **1985**, *23*, 4. (b) Trofimenko, S. *Inorg. Chem.* **1969**, *8*, 2675. (c) Drane, A. S.; McCleverty, J. A. *Polyhedron* **1983**, *2*, 53.
(9) Haworth, J. W.; Heilbron, I. M.; Hey, D. W. *J. Chem. Soc.* **1940**, 358.

Table I. Analytical and Spectroscopic Data for the Ligands

ligand	anal./%[a] C	H	N	EI MS (M^+) m/z	^{1}H NMR/ppm vs Me_4Si[b]
HL^1	77.5 (77.1)	5.1 (5.4)	8.3 (8.2)	171	6.91 (2 H, d, H^2 and H^6), 7.63 (2 H, d, H^3 and H^5), 7.65 (2 H, d, $H^{3'}$ and $H^{5'}$), 8.49 (2 H, d, $H^{2'}$ and $H^{6'}$)
HL^2	78.9 (79.2)	5.7 (5.6)	7.3 (7.1)	197	6.81 (2 H, d, H^2 and H^6), 7.01 (1 H, d, H^7), 7.44 (1 H, d, H^8), 7.47–7.51 (4 H, m, H^3, H^5, $H^{3'}$, and $H^{5'}$), 8.51 (2 H, br s, $H^{2'}$ and $H^{6'}$)
HL^3	79.1 (79.2)	5.5 (5.6)	7.0 (7.1)	197	6.76 (1 H, d, H^6), 7.03 (1 H, s, H^2), 7.09 (1 H, d, H^4), 7.15 (1 H, d, H^7), 7.21 (1 H, t, H^5), 7.47 (1 H, d, H^8), 7.56 (2 H, d, $H^{3'}$ and $H^{5'}$), 8.53 (2 H, d, $H^{2'}$ and $H^{6'}$)
HL^4	79.9 (79.2)	6.0 (5.6)	7.6 (7.1)	197	6.80 (2 H, d, H^2 and H^6), 7.00 (1 H, d, H^7), 7.45 (1 H, d, H^8), 7.48–7.51 (4 H, m, H^3, H^5, $H^{4'}$, and $H^{5'}$), 8.51 (2 H, br s, $H^{2'}$ and $H^{6'}$)
L^5	77.2 (77.8)	5.6 (6.0)	7.5 (7.6)	185	3.84 (3 H, s, OCH_3), 7.06 (2 H, d, H^2 and H^6), 7.69 (2 H, d, H^3 and H^5), 7.71 (2 H, d, $H^{3'}$ and $H^{5'}$), 8.50 (2 H, d, $H^{2'}$ and $H^{6'}$)
L^6	79.8 (79.6)	6.0 (6.2)	6.4 (6.6)	211	3.80 (3 H, s, OCH_3), 6.99 (2 H, d, H^2 and H^6), 7.09 (1 H, d, H^7), 7.50 (1 H, d, H^8), 7.52 (2 H, d, $H^{3'}$ and $H^{5'}$), 7.61 (2 H, d, H^3 and H^5), 8.52 (2 H, br s, $H^{2'}$ and $H^{6'}$)
L^7	79.9 (79.6)	6.0 (6.2)	6.3 (6.6)	211	3.81 (3 H, s, OCH_3), 6.97 (1 H, d, H^6), 7.15–7.30 (2 H, m, H^2 and H^4), 7.37 (1 H, t, H^5), 7.42 (1 H, d, H^7), 7.75 (1 H, d, H^8), 7.92 (2 H, d, $H^{3'}$ and $H^{5'}$), 8.73 (2 H, br s, $H^{2'}$ and $H^{6'}$)
L^8	79.5 (79.6)	6.1 (6.2)	6.5 (6.6)	211	3.79 (3 H, s, OCH_3), 6.99 (2 H, d, H^2 and H^6), 7.10 (1 H, d, H^7), 7.47–7.54 (3 H, m, H^8, $H^{4'}$, and $H^{5'}$), 7.61 (2 H, d, H^3 and H^5), 8.52 (2 H, br s, $H^{2'}$ and $H^{6'}$)

[a] Calculated values in parentheses. [b] All spectra recorded in CD_3OD at 270 MHz.

aqueous methanol to give HL^1–HL^4 in 70–75% yields as pale yellow, crystalline solids.

Analytical, mass spectral, and NMR spectral data for HL^1–HL^4 and L^5–L^8 are given in Table I.

N-Methylation of L^5. This was achieved in 90% yield by reaction of L^5 with a large excess of methyl iodide in CH_2Cl_2 at reflux for 18 h. The mixture was then evaporated to dryness and dissolved in methanol, and KPF_6 was added; [L^5-Me][PF_6] precipitated on cooling and was recrystallized from hot methanol. ^{1}H NMR, CD_3SOCD_3, δ (ppm): 3.89 (3 H, s, OCH_3), 4.28 (3 H, s, NCH_3), 7.19 (2 H, d, J = 8.6 Hz, phenyl H^2 and H^6), 8.11 (2 H, d, J = 8.6 Hz, phenyl H^3 and H^5), 8.44 (2 H, d, J = 5.5 Hz, pyridyl H^3 and H^5), 8.90 (2 H, d, J = 5.5 Hz, pyridyl H^2 and H^6). EI MS: m/z = 185 ($M^+ - CH_3PF_6$). Anal. Calcd for $C_{13}H_{14}NOF_6P$: C, 45.2; H, 4.1; N, 4.1. Found: C, 44.9; H, 4.2; N, 3.9. Mp: 230–232 °C.

Preparations of Mononuclear Complexes 1–4 and 13–16. A mixture of the appropriate ligand (HL^1, HL^2, HL^3, or HL^4; 0.5 mmol), Et_3N (1 cm^3), and [MoL*(NO)Cl_2] (0.197 g, 0.4 mmol, for **1–4**) or [WL*(NO)Cl_2] (0.233 g, 0.4 mmol, for **13–16**) was heated to reflux in toluene (40 cm^3) for 4 h under N_2. The solvent was removed in vacuo, the residue was redissolved in CH_2Cl_2, and the solution was chromatographed on silica with CH_2Cl_2. For the molybdenum complexes **1–4** a small amount of a brown impurity eluted first; after the solvent polarity was increased by adding up to 2% thf (v/v), the desired products then eluted. Complexes **1–4** are deep violet or red-brown, **14** and **16** are pale brown, and **13** and **15** are pale green. The fractions containing the products were concentrated to a volume of ca. 5 cm^3, and the complexes were precipitated by addition of hexane and collected by filtration. Yields were typically 70–75% for **1–4** and 60% for **13–16**.

Preparations of N-Methylated Complexes [9]$^+$–[12]$^+$ and [17]$^+$–[20]$^+$. A mixture of the starting complex (**1–4** or **13–16**; 0.1 g) and methyl iodide (1 cm^3) was heated to reflux in CH_2Cl_2 (20 cm^3) for 18 h. After removal of the solvent in vacuo, the residue was redissolved in MeCN and the solution was chromatographed on a short (12 cm long) column of alumina (Brockmann activity IV) using MeCN (99%)/aqueous KPF_6 (1%) as eluent. The complexes of L^1 ([**9**]$^+$ and [**17**]$^+$) were chromatographed at room temperature; the others were chromatographed between −12 and −14 °C to prevent decomposition on the column. Small amounts of byproducts eluted first before the major product. To the major fraction containing the pure product was added 5 cm^3 of saturated aqueous KPF_6; after evaporation to dryness, the solid residue was extracted from the excess KPF_6 by partitioning between water and CH_2Cl_2. The products were precipitated from the dried ($MgSO_4$), concentrated CH_2Cl_2 solutions by addition of pentane. Complexes **1–4** are brown, **17** and **19** are emerald green, and **18** and **20** are deep yellow-brown. Yields were typically 80–85%.

Preparations of Mononuclear Complexes 5–8. A mixture of the appropriate ligand (L^5, L^6, L^7, or L^8; 0.5 mmol), Et_3N (1 cm^3), and [MoL*(NO)Cl_2] (0.197 g, 0.4 mmol) in toluene (40 cm^3) was heated to reflux for 6 h under N_2. After removal of the solvent in vacuo, the residue was dissolved in CH_2Cl_2 and purified by chromatography on SiO_2 with CH_2Cl_2 as eluent. The major brown fraction was collected in each case and concentrated, and the product was precipitated by addition of hexane. Yields were typically 45% for **5** and 35% for **6–8**; the complexes are brown.

Preparations of Binuclear Complexes 21–24. Complexes **22–24** were prepared in a single step by attachment of both metal centers to the bridging ligand simultaneously. Thus a mixture of the appropriate ligand (HL^2, HL^3, or HL^4; 0.04 g, 0.2 mmol), Et_3N (1 cm^3), and [MoL*(NO)Cl_2] (0.202 g, 0.41 mmol) in toluene (40 cm^3) was heated to reflux for 6 h under N_2. After removal of the solvent in vacuo, the residue was dissolved in CH_2Cl_2 and purified by chromatography on SiO_2 with CH_2Cl_2 as eluent. In each case, the first major fraction (red-brown) contained the desired binuclear complex **22–24**; precipitation of the products from the concentrated CH_2Cl_2 solutions with hexane gave yields of 0.06–0.07 g (30–35%). Second fractions were then separated on increasing the solvent polarity by addition of thf (2%, v/v) to the eluent; these contain the corresponding mononuclear complexes **2–4** which were isolated in approximately 0.05-g (20%) yields. Complex **21** was more readily prepared by attachment of a second metal center to mononuclear complex **1**; thus, a solution of **1** (0.10 g, 0.16 mmol) and [MoL*(NO)Cl_2] (0.079 g, 0.16 mmol) in toluene (40 cm^3) was heated to reflux under N_2 for 6 h. After evaporation of the solvent, the residue was purified by chromatography on SiO_2, the product eluting behind a small fraction of a byproduct. The pure fractions was evaporated to dryness and recrystallized from CH_2Cl_2/hexane, giving **21** in 35% yield. These complexes are deep violet or red-brown.

The structures of all of the new complexes are depicted in Figure 2; analytical and spectroscopic data are given in Table II.

Crystal Structure Determinations. Data were collected using a Siemens R3m/V diffractometer (293 K, Mo Kα X-radiation, graphite monochromator, $\bar{\lambda}$ = 0.710 73 Å). The data were corrected for Lorentz, polarization, and X-ray absorption effects. The structures were solved by conventional heavy-atom or direct methods, and successive difference Fourier syntheses were used to locate all non-hydrogen atoms. Final refinements by full-matrix least-squares procedures were performed on a μ-Vax computer with the SHELXTL system of programs.[11] Scattering factors with corrections for anomalous dispersion were taken from ref 12. Full listings of bond distances and angles and thermal parameters have been deposited with the Cambridge Crystallographic Data Centre, University Chemical Laboratory, Lensfield Road, Cambridge CB2 1EW, U.K. Structure factors are available from the authors.

(10) Dietrich-Buchecker, C.; Sauvage, J.-P. *Tetrahedron* **1990**, *46*, 503.

(11) Sheldrick, G. M. SHELXTL programs for use with a Siemens X-ray System. University of Cambridge, 1976; updated, University of Göttingen, 1981.

(12) *International Tables for X-Ray Crystallography*; Kynoch Press: Birmingham, England, 1974; Vol. 4.

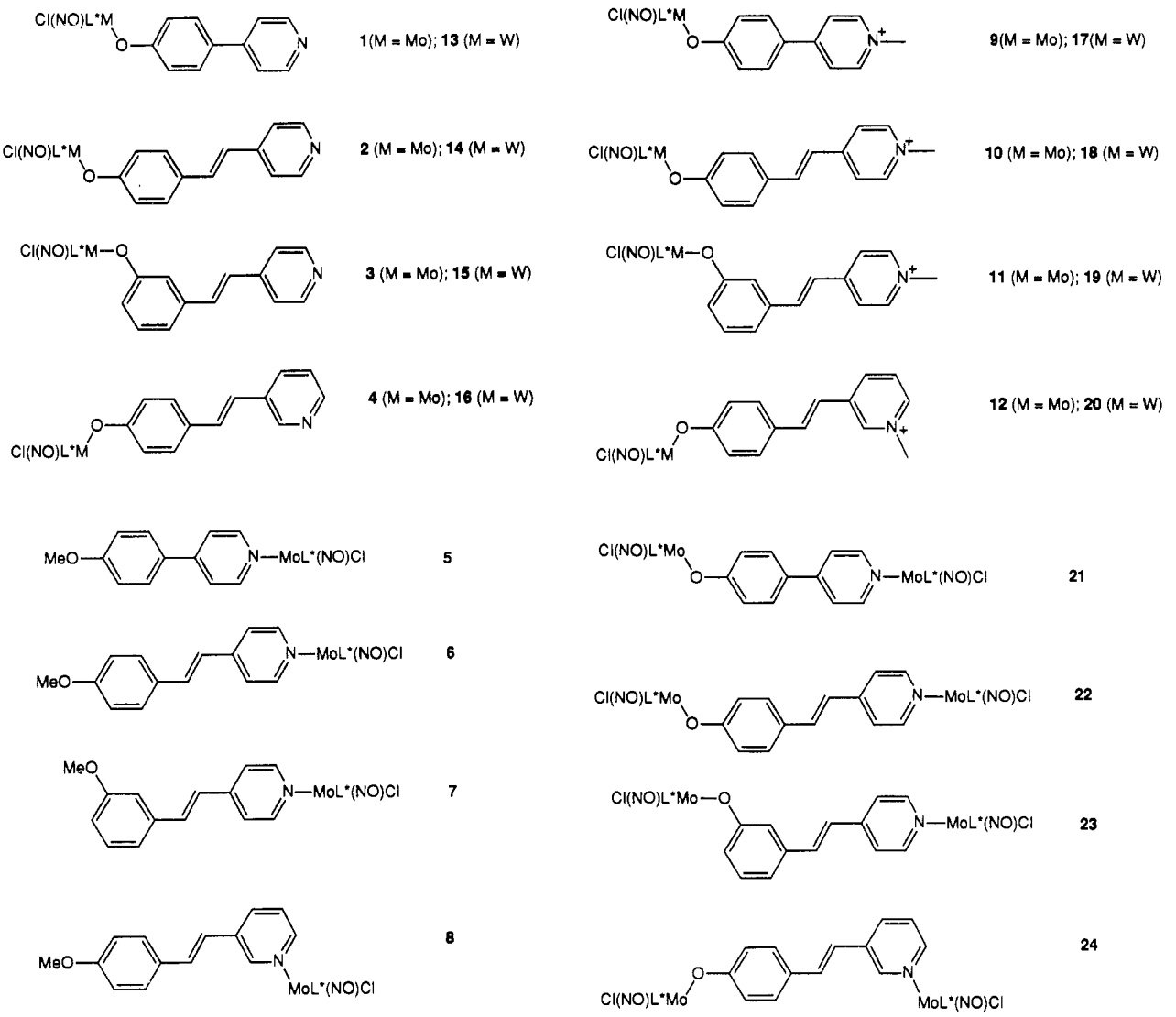

Figure 2. Structures of the new complexes.

Structure Determination of [MoL*(NO)ClL^5] (5). Crystals of **5** were grown from CH_2Cl_2/*n*-hexane as dark green plates. The selected crystal had dimensions of ca. 0.40 × 0.29 × 0.14 mm and was mounted in a sealed glass capillary under N_2 saturated with CH_2Cl_2. Of the 6207 data collected (Wyckoff ω-scans, $2\theta \leq 50°$), 4403 unique data had $F \geq 5\sigma(F)$, and only these were used for structure solution and refinement. An empirical absorption correction was applied using a method based upon azimuthal scan data.

Crystal Data for 5: $C_{27}H_{33}BClMoN_8O_2 \cdot CH_2Cl_2$, $M = 728.7$, triclinic, space group $P\bar{1}$, $a = 10.641(4)$ Å, $b = 10.893(4)$ Å, $c = 14.865(7)$ Å, $\alpha = 96.43(3)°$, $\beta = 98.00(3)°$, $\gamma = 98.56(3)°$, $V = 1672(1)$ Å^3, $Z = 2$, $D_c = 1.45$ g cm^{-3}, $F(000) = 746$, μ(Mo Kα) = 6.7 cm^{-1}.

All non-hydrogen atoms were refined with anisotropic thermal parameters. Methyl, pyrazolyl, BH, and phenyl hydrogen atoms were included in calculated positions (C–H = 0.96 Å) with fixed isotropic thermal parameters (U_{iso} = 0.08 Å^2). Refinement converged at R = 0.066 (R_w = 0.067) with a weighting scheme of the form $w^{-1} = [\sigma^2(F) + 0.0014|F|^2]$. The final electron density difference synthesis showed no peaks >1.30 or <–1.74 e Å^{-3}, these being in the vicinity of the CH_2Cl_2 solvent molecule.

The Cl and NO ligands are mutually disordered. Approximately 76% of the time these ligands occupy the sites shown in Figure 6, and the remainder of the time their sites are interchanged. There is no evidence of disorder in the remainder of the complex. In particular, the atoms of the biphenylene ring system are well defined with moderate anisotropic thermal parameters.

Structure Determination of [L^5-Me][PF$_6$]. Crystals of [L^5-Me][PF$_6$] were grown from methanol as colorless prisms. The selected crystal had dimensions of ca. 0.60 × 0.55 × 0.50 mm and was mounted in a sealed glass capillary under N_2. Of the 3847 data collected (Wyckoff ω-scans, $2\theta \leq 50°$), 1408 unique data had $F \geq 3\sigma(F)$, and only these were used for structure solution and refinement. An empirical absorption correction was applied using a method based upon azimuthal scan data.

Crystal Data for [L^5-Me][PF$_6$]: $C_{13}H_{14}F_6NOP$, $M = 345.2$, monoclinic, space group $P2_1/n$, $a = 6.514(2)$ Å, $b = 23.026(6)$ Å, $c = 10.299(3)$ Å, $\beta = 103.46(2)°$, $V = 1502.4(8)$ Å^3, $Z = 4$, $D_c = 1.53$ g cm^{-3}, $F(000) = 704$, μ(Mo Kα) = 2.5 cm^{-1}.

All non-hydrogen atoms were refined with anisotropic thermal parameters. Methyl and phenyl hydrogen atoms were included in calculated positions (C–H = 0.96 Å) with fixed isotropic thermal parameters (U_{iso} = 0.08 Å^2). Refinement converged at R = 0.105 (R_w = 0.107) with a weighting scheme of the form $w^{-1} = [\sigma^2(F) + 0.0003|F|^2]$. The final electron density difference synthesis showed no peaks >0.62 or <–0.76 e Å^{-3}. Several crystals were examined prior to data collection. All were found to diffract poorly, and representative intensities had broad peak profiles which may have led to some resolution problems for stronger low-angle data. These factors, together with the large thermal motion observed in the [PF$_6$]$^-$ counterion, no doubt contribute to the poor overall level of refinement.

Results and Discussion

Ligand Syntheses. Synthesis of L^5 was accomplished by two different methods, both adapted from published procedures used to prepare similar compounds.[13,14] In the first method, pyridine is activated to nucleophilic attack by N-acylation with methyl chloroformate;[13] the presence of a catalytic amount of CuI ensures

(13) Comins, D. L.; Abdullah, A. H. *J. Org. Chem.* **1982**, *47*, 4375.

Table II. Spectroscopic and Analytical Data for the New Complexes

complex	anal./%[a] C	H	N	ν(NO)/cm^{-1}	FABMS[b] m/z and assignments[c]
1	50.3 (49.7)	5.1 (4.8)	17.5 (17.8)	1686	630 (M^+), 595 ($M^+ - Cl$), 460 [MoL*(NO)Cl]
2	52.0 (51.4)	5.2 (4.9)	16.8 (17.1)	1684	656 (M^+), 619 ($M^+ - Cl$), 460 [MoL*(NO)Cl]
3	51.7 (51.4)	4.9 (4.9)	16.9 (17.1)	1685	657 (M^+), 619 ($M^+ - Cl$), 460 [MoL*(NO)Cl]
4	51.8 (51.4)	5.0 (4.9)	17.0 (17.1)	1684	657 (M^+), 619 ($M^+ - Cl$), 460 [MoL*(NO)Cl]
5	49.9 (50.4)	5.4 (5.2)	17.0 (17.4)	1607	644 (M^+), 610 ($M^+ - Cl$), 460 [MoL*(NO)Cl]
6	51.6 (52.0)	5.1 (5.3)	16.9 (16.7)	1603	672 (M^+), 637 ($M^+ - Cl$), 461 [MoL*(NO)Cl]
7	52.6 (52.0)	5.0 (5.3)	16.4 (16.7)	1604	671 (M^+), 636 ($M^+ - Cl$), 460 [MoL*(NO)Cl]
8	52.3 (52.0)	5.2 (5.3)	16.5 (16.7)	1604	671 (M^+), 637 ($M^+ - Cl$), 460 [MoL*(NO)Cl]
9	41.3 (41.1)	4.4 (4.2)	14.1 (14.2)	1684	644 ($M^+ - PF_6$), 628 ($M^+ - CH_3 - PF_6$), 609 ($M^+ - CH_3 - PF_6 - Cl$)
10	44.0 (43.6)	4.6 (4.4)	13.9 (14.0)	1688	672 ($M^+ - PF_6$), 636 ($M^+ - PF_6 - Cl$), 460 [MoL*(NO)Cl]
11	43.0 (43.6)	4.4 (4.4)	14.1 (14.0)	1689	671 ($M^+ - PF_6$), 637 ($M^+ - PF_6 - Cl$), 461 [MoL*(NO)Cl]
12	43.8 (43.6)	4.3 (4.4)	13.9 (14.0)	1688	671 ($M^+ - PF_6$), 638 ($M^+ - PF_6 - Cl$), 460 [MoL*(NO)Cl]
13	44.0 (43.6)	4.3 (4.2)	15.3 (15.6)	1645	717 (M^+), 681 ($M^+ - Cl$), 546 [WL*(NO)Cl]
14	45.9 (45.3)	4.5 (4.3)	14.9 (15.1)	1642	743 (M^+), 707 ($M^+ - Cl$)
15	46.0 (45.3)	4.5 (4.3)	15.0 (15.1)	1645	742 (M^+), 707 ($M^+ - Cl$), 544 [WL*(NO)Cl]
16	45.4 (45.3)	4.5 (4.3)	15.2 (15.1)	1645	743 (M^+), 708 ($M^+ - Cl$), 545 [WL*(NO)Cl]
17	36.5 (37.0)	3.9 (3.8)	12.9 (12.8)	1644	731 ($M^+ - PF_6$), 714 ($M^+ - CH_3 - PF_6$), 548 [WL*(NO)Cl]
18	39.6 (39.2)	4.0 (4.0)	12.5 (12.6)	1646	758 ($M^+ - PF_6$), 722 ($M^+ - PF_6 - Cl$), 544 [WL*(NO)Cl]
19	39.6 (39.2)	4.1 (4.0)	12.7 (12.6)	1647	757 ($M^+ - PF_6$), 721 ($M^+ - PF_6 - Cl$), 545 [WL*(NO)Cl]
20	39.9 (39.2)	4.2 (4.0)	12.5 (12.6)	1646	758 ($M^+ - PF_6$), 721 ($M^+ - PF_6 - Cl$), 544 [WL*(NO)Cl]
21	46.0 (45.3)	5.2 (4.8)	18.9 (19.3)	1687, 1611	1088 (M^+), 1052 ($M^+ - Cl$), 629 [M^+ - MoL*(NO)Cl]
22	47.0 (46.4)	5.0 (4.9)	19.0 (18.9)	1685, 1607	1115 (M^+), 1079 ($M^+ - Cl$), 655 [M^+ - MoL*(NO)Cl]
23	46.9 (46.4)	5.1 (4.9)	18.7 (18.9)	1686, 1608	1113 (M^+), 1078 ($M^+ - Cl$), 655 [M^+ - MoL*(NO)Cl]
24	47.0 (46.4)	5.0 (4.9)	18.7 (18.9)	1684, 1608	1115 (M^+), 1078 ($M^+ - Cl$), 655 [M^+ - MoL*(NO)Cl]

[a] Calculated values in parentheses. [b] All FAB mass spectra run with 3-nitrobenzyl alcohol as matrix. [c] The position of the most intense peak of the cluster is quoted in each case. Due to the presence of numerous isomers of similar abundance for Mo and W, and possible protonation by the matrix, the quoted values may differ slightly from the expected values calculated from the most abundant isotopes.

attack of *p*-MeO(C_6H_4)MgBr at the 4-position of the pyridine ring to give 4-(4-methoxyphenyl)-1,4-dihydropyridine. This is not isolated, but rearomatized directly with $KMnO_4$ to give L^5 in 60% yield. The second method is a cross-coupling of *p*-MeO-(C_6H_4)MgBr with 4-bromopyridine using [Ni(PPh_3)$_2Cl_2$] as catalyst,[14] and gives L^5 in 74% yield. L^5 was prepared previously by photolysis of 4-iodopyridine in anisole[15] and by reaction of diazotized 4-methoxyaniline with pyridine,[9] but both of these methods give mixtures of 2-, 3-, and 4-substituted isomers which require chromatographic separation and give low yields. There is also a report of the preparation of L^5 in 75% yield from the palladium-catalyzed cross-coupling of diethyl(4-pyridyl)borane with 4-bromoanisole,[16] but this requires conversion of 4-bromopyridine to diethyl(4-pyridyl)borane in a separate step. Both of the methods we have developed are simple and convenient; although method B has the slightly better yield, method A avoids the use of 4-bromopyridine, which is relatively expensive and requires careful handling due to its tendency to polymerize when warm, and we have found it to be the most convenient route to L^5. Demethylation of L^5 to HL^1 was achieved in 70% yield with molten pyridinium chloride.[10] Although HL^1 was recently prepared by other routes,[17,18] no coordination chemistry has hitherto been reported.

L^6, L^7, and L^8 were all prepared by deprotonation of the appropriate methylpyridine with LDA, followed by reaction with the appropriate isomer of methoxybenzaldehyde; the intermediate alcohol was dehydrated with $POCl_3$ in pyridine. This method is based on a similar published procedure by which 2 equiv of the monoanion of 4,4′-dimethylbipyridine was condensed with terephthaldehyde.[19] Demethylation of these to give HL^2–HL^4, respectively, was again performed with pyridinium chloride.[10]

Preparations of Complexes. Reaction of HL^1–HL^4 with 1 equiv of [ML*(NO)Cl_2] (M = Mo, W) in toluene at reflux, in the presence of Et_3N, resulted in formation of the mononuclear complexes **1–4** (M = Mo) and **13–16** (M = W). In each case, the phenoxide terminus of the ligand is attached to the 16-electron metal center and the pyridyl group is pendant. These reactions are apparently controlled by the difference in reaction rate between the anionic phenolate and the neutral pyridine with the electron-deficient [ML*(NO)Cl_2]. Attachment of the pyridyl terminus to molybdenum can only be achieved if the phenol is protected, as in L^5–L^8; thus, reaction of [MoL*(NO)Cl_2] with L^5–L^8 in toluene at reflux in the presence of Et_3N produces **5–8**, which have pendant methoxyphenyl groups. These are 17-electron complexes; attachment of the pyridyl ligand to the molybdenum is accompanied by a one-electron reduction. The reducing agent is probably Et_3N, since in its absence the yields are considerably reduced, and the propensity of amines to act as hydridic reducing agents has been well established.[20] Attempts to attach L^5–L^8 to a tungsten center were unsuccessful.

Binuclear complexes **21–24** were prepared by one of two routes. Complex **21** was best prepared in a stepwise manner, by attachment of a second MoL*(NO)Cl moiety to the pendant pyridyl group of **1**. Complexes **22–24** were prepared in a single step, by reaction of the free ligands HL^2–HL^4 with 2 equiv of [MoL*(NO)Cl_2] in the presence of Et_3N; the binuclear products could be chromatographically separated from the mononuclear complexes **2–4**, which also form, since the binuclear complexes elute more quickly than the mononuclear complexes which have pendant polar groups. All binuclear complexes contain a 16-electron molybdenum center at the phenolate terminus of the bridging ligand and a 17-electron molybdenum center at the pyridyl terminus. Finally, mononuclear complexes **1–4** and **13–16** could be N-methylated at the pendant pyridyl group with methyl iodide, to give [**9**]$^+$–[**12**]$^+$ and [**17**]$^+$–[**20**]$^+$, respectively, in high yield as their hexafluorophosphate salts. The structures of the complexes are summarized in Figure 2.

(14) (a) Sauvage, J.-P.; Ward, M. D. *Inorg. Chem.* **1991**, *30*, 3869. (b) Hacksell, U.; Arvidsson, L.-E.; Svennson, U.; Nilsson, J. L. G.; Sanchez, D.; Wikstrom, H.; Linberg, P.; Hjorth, S.; Carlsson, A. *J. Med. Chem.* **1981**, *24*, 1475.
(15) Ohkura, K.; Seki, K.; Terashima, M.; Kanaoka, Y. *Tetrahedron Lett.* **1989**, *30*, 3433.
(16) Ishikura, M.; Ohta, T.; Terashima, M. *Chem. Pharm. Bull.* **1985**, *33*, 4755.
(17) Singh, B.; Lesher, C. Y. *J. Heterocycl. Chem.* **1991**, *28*, 933.
(18) Alvarez, C.; Delgado, F.; Garciá, O.; Medina, S.; Márquez, C. *Synth. Commun.* **1991**, *21*, 619.
(19) Shaw, R. J.; Webb, R. T.; Schmehl, R. H. *J. Am. Chem. Soc.* **1990**, *112*, 1117.
(20) Kaitmazova, G. S.; Gambaryan, N. P.; Rokhlin, E. M. *Russ. Chem. Rev. (Engl. Transl.)* **1989**, *58*, 1145.

Table III. Electrochemical and EPR Data for the New Complexes

	electrochemical data[a]					EPR data[b]		
complex	16/17e Mo[c]	17/16e Mo[d]	17/18e Mo[e]	16/17e W[f]	Me–Pyr[g]	g_{av} (293 K)	A_{av}/mT[h]	$g_{\|}$, $g_{\perp}$ (77 K)
1	–0.70 (75)							
[**1**]$^{-}$[i]						1.969	5.1	1.997, 1.914
2	–0.72 (80)							
[**2**]$^{-}$[i]						1.969	5.1	1.997, 1.914
3	–0.71 (90)							
[**3**]$^{-}$[i]						1.969	5.1	1.996, 1.914
4	–0.72 (80)							
[**4**]$^{-}$[i]						1.969	5.1	1.997, 1.915
5		+0.11 (70)	–1.87 (100)			1.978	5.0	
6		+0.10 (110)	–1.76 (130)			1.978	4.9	2.004, 1.925
7		+0.11 (140)	–1.77 (140)			1.978	4.9	2.003, 1.925
8		+0.11 (125)	–1.77 (135)			1.978	4.9	2.004, 1.925
[**9**]$^{+}$	–0.58 (80)				–1.90			
9[j]						1.970	5.1	1.997, 1.915
[**10**]$^{+}$	–0.64 (100)				–1.75			
10[j]						1.969	5.1	1.996, 1.914
[**11**]$^{+}$	–0.70 (100)				–1.57			
11[j]						1.969	5.1	1.996, 1.914
[**12**]$^{+}$	–0.64 (95)				–1.68			
12[j]						1.969	5.1	1.993, 1.914
13				–1.22 (90)				
14				–1.24 (105)				
15				–1.28 (110)				
16				–1.25 (100)				
[**17**]$^{+}$				–1.11 (105)	–1.92			
[**18**]$^{+}$				–1.16 (80)	–1.70			
[**19**]$^{+}$				–1.26 (100)	–1.62			
[**20**]$^{+}$				–1.17 (100)	–1.71			
21	–0.65 (90)	+0.12 (80)	–2.00 (180)			1.979	4.9	2.004, 1.925
[**21**]$^{-}$[j]						1.973	2.6	
22	–0.69 (75)	+0.11 (95)	–1.89 (140)			1.978	4.9	2.004, 1.925
[**22**]$^{-}$[j]						1.973	2.5	
23	–0.74 (90)	+0.11 (85)	–1.81 (120)			1.978	4.9	2.004, 1.926
[**23**]$^{-}$[j]						1.973	2.5	
24	–0.69 (75)	+0.11 (90)	–1.86 (140)			1.978	4.9	2.004, 1.925
[**24**]$^{-}$[j]						1.973	2.5	

[a] Cyclic voltammograms were recorded in MeCN at a scan rate of 0.2 V s^{-1}. Potentials are vs the ferrocene/ferrocenium couple, Fc/Fc^{+}; peak–peak separations ΔE_p are given in parentheses. [b] EPR spectra recorded in CH_2Cl_2/thf (1:1, v/v). [c] Potentials for the 16e → 17e reduction of Mo–phenolate complexes. [d] Potentials for the 17e → 16e oxidation of Mo–pyridyl complexes. [e] Potentials for the 17e → 18e reduction of Mo–pyridyl complexes. [f] Potentials for the 16e → 17e reduction of W–phenolate complexes. [g] Potentials for the reduction of methylpyridinium groups. Since some of these are not fully reversible (return wave smaller than outward wave), the peak potential for the outward wave is given in each case to facilitate comparison. [h] Due to second-order coupling effects, the lines in the spectrum are not quite equally spaced; the quoted values are therefore an average and are accurate to ±0.05 mT. [i] 17-electron Mo–phenolate complexes produced by in situ reduction of 16-electron complexes **1–4** and [**9**]$^{+}$–[**12**]$^{+}$ with cobaltocene. [j] 34-electron (17 + 17) binuclear Mo complexes produced by in situ reduction of 33-electron (17 + 16) complexes **21–24** with cobaltocene.

All of the complexes were satisfactorily characterized by elemental analysis and FAB mass spectrometry (Table II). Confirmation of the formation of binuclear complexes **21–24** is provided by the position of the NO stretching frequencies in their IR spectra. The [MoL*(NO)Cl(pyridyl)] and [MoL*(NO)Cl(phenolate)] chromophores have characteristic ν_{NO} frequencies of about 1685 and 1608 cm^{-1}, respectively, in their mononuclear complexes;[21] the binuclear molybdenum complexes have two distinct ν_{NO} bands, one at each of these frequencies. In addition, the diamagnetic complexes **1–4**, [**9**]$^{+}$–[**12**]$^{+}$, **13–16**, and [**17**]$^{+}$–[**20**]$^{+}$ gave ^{1}H NMR spectra consistent with the formulations. All show resonances of total intensity 8 H between 7 and 9 ppm from the aromatic ligands, three signals (each intensity 1 H) close to 6 ppm due to the pyrazolyl protons, up to six signals (total intensity 18 H) between 2 and 3 ppm from the pyrazolyl methyl groups, and (for the N-methylated complexes [**9**]$^{+}$–[**12**]$^{+}$ and [**17**]$^{+}$–[**20**]$^{+}$) singlets (intensity 3 H) near 4.5 ppm.

Electrochemistry. The electrochemical results are summarized in Table III. Comparison of the data for **1–4** with those for their N-methylated analogues [**9**]$^{+}$–[**12**]$^{+}$ gives a good indication of how effectively these ligands can mediate electronic interactions between their ends. First, N-methylation of the pendant pyridyl groups of **1–4** results in an anodic shift of the characteristic[22] 16-electron to 17-electron metal-centered reductions by 120, 80, 10, and 80 mV, respectively, in [**9**]$^{+}$–[**12**]$^{+}$. We conclude that L^1, despite the potentially free rotation about the central C–C bond, allows a stronger interaction between the metal center and the N-methylpyridinium group than do L^2–L^4, which are all constrained to be planar by the presence of an ethene linkage between the aromatic rings. This is in marked contrast to the behavior of mononuclear polypyridine–ruthenium(II) complexes with 4,4′-bipyridyl ligands, where N-methylation of the pendant pyridyl groups results in an anodic shift of the Ru^{II}/Ru^{III} redox couples by just 20 mV per methylpyridinium group.[23] An explanation for the strong interaction across L^1 is provided by considering the different canonical forms of the methylated ligand; transfer of charge from the negatively-charged phenolate to the methylpyridinium group results in a quinonoidal structure (Figure 3a). This is likely to be planar and will result in a decrease of electron density at the metal center (thereby facilitating the reduction) and an increase of electron density in the methylpyridinium ring (thereby making the reduction more difficult). Since

(21) Al Obaidi, N.; Chaudhury, M.; Clague, D.; Jones, C. J.; Pearson, J. C.; McCleverty, J. A.; Salam, S. S. *J. Chem. Soc., Dalton Trans.* **1987**, 1733.

(22) Charsley, S. M.; Jones, C. J.; McCleverty, J. A.; Neaves, B. D.; Reynolds, S. J.; Denti, G. *J. Chem. Soc., Dalton Trans.* **1988**, 293.

(23) (a) Hayes, M. A.; Meckel, C.; Schatz, E.; Ward, M. D. *J. Chem. Soc., Dalton Trans.* **1992**, 703. (b) Sullivan, B. P.; Abruna, H.; Finklea, H. O.; Salmon, D. J.; Nagle, J. K.; Meyer, T. J.; Sprintschnik, H. *Chem. Phys. Lett.* **1978**, *58*, 389.

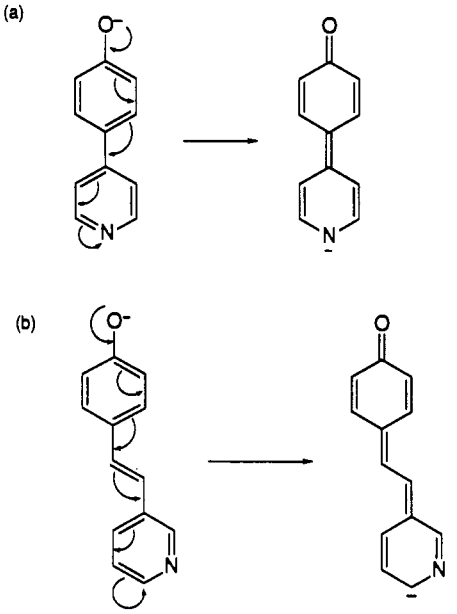

Figure 3. Alternative canonical forms of the bridging ligands: (a) L^1 (L^2 will be similar); (b) L^4.

L^1 is expected to be planar in $[9]^+$, the weaker interaction of 80 mV across L^2 (compare **2** and $[10]^+$), for which a similar quinonoidal structure can be envisaged, may be ascribed to the increased separation of the metal centers as a result of the additional ethene spacer. This is similar to the behavior observed for ruthenium complexes of α,ω-bis(4-pyridyl)polyenes, where increasing the number of double bonds in the "wire" results in a steady decrease in the metal–metal interaction as measured by cyclic voltammetry.[4]

The communicative properties of L^3 and L^4 can be explained likewise. Due to the position of the oxygen atom in L^3, meta to the conjugated linker, no resonance structure can be drawn in which the negative charge can leave the phenolate ring; it is trapped, and the phenolate and methylpyridinium groups are effectively isolated from each other. The small anodic shift of 10 mV (which is at the limit of significance) for the metal reduction in $[11]^+$ compared to **3** may be ascribed to a simple through-space Coulombic effect of a nearby positive charge. For the same reason, the methylpyridinium group in $[11]^+$ is the easiest to reduce as the positive charge is localized. The electrochemical interaction across L^4 (compare **4** and $[12]^+$) is identical to that of L^2; the para position of the phenolate oxygen means that the negative charge may be delocalized out of the aromatic ring, making the metal center 80 mV easier to reduce. However, in the resultant canonical form of L^4 (Figure 3b), the negative charge can only reside adjacent to the positively-charged N atom, rather than directly neutralizing it (as in the extreme forms of L^1 and L^2).

The same pattern is evident from comparison of the tungsten complexes **13–16** with their N-methylated counterparts $[17]^+$–$[20]^+$. The anodic shifts of the metal centers caused by methylation of L^1–L^4 are 110, 80, 20, and 80 mV, respectively, in excellent agreement with the results from the molybdenum complexes, and again these values are mirrored by the cathodic shifts in the reduction potentials of the methylpyridinium groups.

The magnitudes of electrochemical interactions in the binuclear complexes **21–24** may be determined by comparison with the properties of the mononuclear components **1–4** and **5–8**. A representative example is shown in Figure 4. Whereas the difference between the reduction potentials of **1** and **5** is 1.17 V, the presence of a direct link between the same two components in **21** results in a $\Delta(E_{1/2})$ value of 1.35 V for the two reductions, i.e. an increase of 180 mV. The increases in $\Delta(E_{1/2})$ values for **22–24** are 160, 10, and 120 mV. This again places the ligands

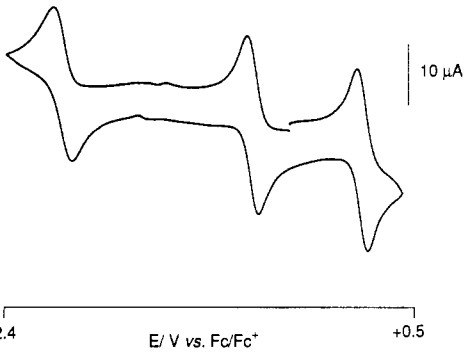

Figure 4. Cyclic voltammogram of **21** in MeCN at 0.2 V s^{-1} at a Pt bead working electrode, showing (from left to right) the 17e/18e reduction of the pyridyl-substituted Mo center, the 16e/17e reduction of the phenolate-substituted Mo center, and the 17e/16e oxidation of the pyridyl-substituted Mo center.

in the same order with regard to their ability to mediate electronic interactions, i.e. $L^1 > L^2 > L^4 > L^3$. As with the N-methylated complexes, the changes in redox potentials may be accounted for by the extent to which a quinonoidal canonical form contributes to the structure of the bridging ligand. In this respect, attachment of a metal complex to the pendant pyridyl N atoms of **1–4** appears to have a similar electrochemical effect on the group at the phenolate terminus as does N-methylation; this analogy has been commented on before.[24]

It is also instructive to observe what happens to the oxidative processes in the binuclear complexes. The oxidation potentials for the 17-electron molybdenum centers of **5–8** are all at about +0.11 V vs Fc/Fc^+. In the binuclear complexes **21–24**, of which they are components, these processes are essentially unchanged. This suggests that the oxidation processes involve predominantly metal-centered orbitals and are therefore relatively insensitive to the presence of substituents at the other end of the bridging ligand, whereas the orbitals involving the reductions are substantially delocalized onto the bridging ligand and therefore subject to considerable perturbation by remote substituents. This is similar to the behavior of some recently-reported binuclear ruthenium–polypyridyl complexes which consist of two $[Ru(bipy)_3]^{2+}$ and two $[Ru(terpy)_2]^{2+}$ units, respectively, joined "back-to-back" via a 4,4′-bipyridyl linkage.[3i,j] In each case, the two oxidations (predominantly metal-localized) are only ca. 56 mV apart, whereas the first two reductions (predominantly centered on the bridging ligand) are ca. 300 mV apart.

EPR Spectroscopy. The presence of metal–metal interactions across L^1–L^4 may also be observed in the EPR spectra, whose data are summarized in Table III. The 17-electron [MoL*(NO)Cl(pyridyl)] centers of **5–8** have characteristic signals at room temperature at $g_{av} = 1.978 \pm 0.001$, with a hyperfine coupling constant of ca. 5.0 mT and all of the components expected from the different Mo isotopes in their natural abundance. Molybdenum has two spin-active isotopes, $^{95}_{42}$Mo and $^{97}_{42}$Mo (natural abundances 15.72% and 9.46%), which have very similar nuclear magnetic moments of –0.913 and –0.933 μ_N. The hyperfine coupling constants are therefore sufficiently similar that two sets of signals cannot be distinguished, and the spectra can be adequately explained simply by considering the 25.2% of the signal intensity is split into a 1:1:1:1:1:1 sextet with the other 74.8% as a central single peak. A representative spectrum is shown in Figure 5a. Virtually identical spectra were observed for **21–24**, indicating that the unpaired electron is trapped at the pyridyl-substituted molybdenum center, which is to be expected considering the difference in redox potentials (ca. 0.8 V) between the two sites in each binuclear complex. The 16-electron [MoL*(NO)Cl(phenolate)] centers of **1–4** and $[9]^+$–$[12]^+$ could be readily reduced in situ with cobaltocene to give the corresponding

(24) Gillard, R. D. *Comments Inorg. Chem.* **1986**, *5*, 175.

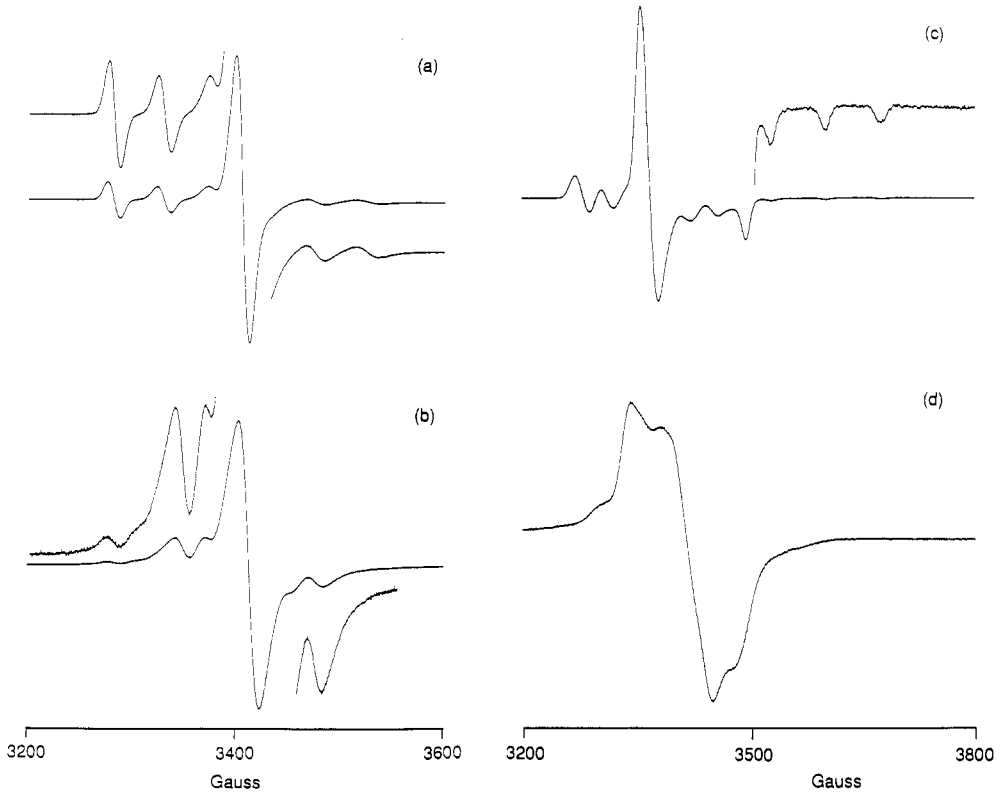

Figure 5. EPR spectra of (a) a valence-trapped 17e–16e complex (**21**) at room temperature, (b) the 17e–17e species [**21**]$^-$ produced by addition of cobaltocene to a solution of **21** in the EPR tube at room temperature, (c) **21** as a frozen glass at 77 K, and (d) [**21**]$^-$ as a frozen glass at 77 K.

17-electron species, which all have a characteristic signal at g_{av} = 1.969 ± 0.001, also with a hyperfine coupling constant of ca. 5 mT and all the expected components from the different Mo isotopes. These spectra look the same as those of the 17-electron pyridyl-substituted complexes (Figure 5a) apart from the slightly lower g value.

One-electron reductions of **21–24** with cobaltocene affords the 17e–17e species [**21**]$^-$–[**24**]$^-$. These are biradicals having 17 electrons at both the pyridyl-substituted and phenolate-substituted molybdenum termini, with the two unpaired electrons in redox levels ca. 0.8 V apart. Despite the energy gap between the unpaired electrons, the room-temperature solution spectra (for example, Figure 5b) indicate a change from valence-trapped to delocalized on the EPR time scale, with the two unpaired electrons in fast exchange across the bridging ligand. Three separate features of the spectra confirm this.

(i) A single signal is observed in each case at g_{av} = 1.973, midway between the values expected for each component (**1–4** and **5–8**) in isolation (1.969 and 1.978, respectively). At a microwave frequency of ca. 9.2 GHz, the lowest rate of electron exchange between the two metals necessary to give an averaged signal is given by $v = [(1.978 - 1.969)/1.973] \times (9.2 \times 10^9) \approx 4 \times 10^7$ s^{-1}. Studies of electron transfer across saturated hydrocarbon bridges have shown transfer rates in the region 10^6–10^9 s^{-1},[25] the higher end of which is comfortably above our required minimum.

(ii) The hyperfine splitting to molybdenum is halved from 5.0 mT to around 2.5 mT. As with [{Mo(NO)L*Cl}$_2$(μ-4,4′-bipy)], this is consistent with both electrons coupling to both metal centers with $|J| \gg A_0$ (where $|J|$ is the exchange integral and A_0 is the hyperfine interaction); in such cases, the hyperfine splitting is predicted to be $0.5(A_0/g\beta)$, that is, half the value found in the spectra of the mononuclear components.[26]

(iii) The components expected from coupling to two molybdenum sites with the Mo isotopes in their natural abundance are present. Assuming, as before, that the two spin-active isotopes have essentially the same coupling constant, we would expect a superposition of a central singlet, a 1:1:1:1:1:1 sextet, and a 1:2:3:4:5:6:5:4:3:2:1 11-fold multiplet. Not all of these are resolved, and this simple simulation does not take anisotropic effects into account which broaden the spectra at higher fields and perturb some of the line intensities, but enough of the weak, outlying components are present to confirm the assignment. At 77 K, all of the species with an isolated 17-electron center give axial spectra (Figure 5c) whose two g values are included in Table III; in all cases, $(2g_{\parallel} + g_{\perp})/3 = g_{av}$. Spectra of the 17e–17e biradicals at 77 K are however unhelpful, being broad and featureless. Figure 5d shows a typical example.

It is noteworthy that this fast exchange occurs even across L[3], whose components are electrochemically isolated from each other; similar behavior was observed in the symmetrical 34-electron complex [{Mo(NO)L*Cl}$_2$(μ-bpa)] [bpa = 1,2-bis(4-pyridyl)-ethane] which contains a saturated –CH_2CH_2– bridge, although in this case there was a significant electrochemical interaction (105 mV splitting of the redox potentials) between the two metal centers.[5] Although [**21**]$^-$–[**24**]$^-$ are formally triplets, no half-field resonance (double-quantum transition) was observed in any case either at room temperature or at 77 K, which may be ascribed to the intermetallic separation involved.[5] Despite the asymmetry of [**21**]$^-$–[**24**]$^-$, there is no barrier to double electron exchange arising from reorganization of the metal coordination spheres, since both metal centers formally possess 17 electrons before and after exchange. To our knowledge, these are the first examples of fast exchange in asymmetric biradical, bimetallic systems. They present interesting possibilities for signaling devices, since it is possible for a reversible modification of one metal center to change the electronic properties of (i.e. send a signal to) a second metal center at the other end of a long molecular wire such as a polyene chain. It will be of interest to see over what distances this interaction can be maintained.

(25) (a) Miller, J. R.; Calcaterra, L. T.; Closs, G. L. *J. Am. Chem. Soc.* **1984**, *106*, 3047. (b) Closs, G. L.; Piotrowiak, P.; MacInnis, J. M.; Fleming, S. R. *J. Am. Chem. Soc.* **1988**, *110*, 2652.

(26) Reitz, D. C.; Weissmann, S. I. *J. Chem. Phys.* **1960**, *33*, 700.

Table IV. Electronic Spectral Data for the New Complexes in CH_2Cl_2

complex	λ_{max}/nm ($\epsilon/10^3$ M^{-1} cm^{-1})				
1	276 (17)[a]	486 (8.3)[b]			
2	323 (28)[a]	529 (9.0)[b]			
3	305 (20)[a]	459 (3.9)[b]			
4	322 (30)[a]	530 (9.8)[b]			
5		309 (18)[a]	380 (3.2)		504 (1.6)[c]
6	287 (9.6)	354 (26)[a]	426 (3.1)	472 (3.1)	558 (1.2)[c]
7	281 (9.6)	357 (29)[a]	424 (3.6)	472 (3.5)	559 (1.3)[c]
8	282 (8.9)	356 (25)[a]	426 (3.1)	471 (3.1)	560 (1.2)[c]
9	250 (24)	352 (18)[d]	410 (sh)[b]		
10	260 (sh)	405 (27)[d]	470 (sh)[b]		
11		364 (25)[d]	480 (sh)[b]		
12	260 (sh)	405 (30)[d]	480 (sh)[b]		
13	280 (23)	397 (9.0)[a]	605 (0.3)[e]		
14	326 (25)	420 (sh)[a]	630 (sh)[e]		
15	303 (25)	390 (sh)[a]	591 (0.2)[e]		
16	319 (29)	425 (13)[a]	630 (sh)[e]		
17		390 (19)[d]	627 (0.3)[e]		
18	250 (19)	426 (30)[d]	630 (sh)[e]		
19	250 (sh)	365 (32)[d]	587 (0.4)[e]		
20	250 (17)	431 (29)[d]	608 (0.5)[e]		
21	286 (18)[a]	317 (20)[a]	482 (8.8)[b]		
22	290 (10)[a]	358 (22)[a]	518 (8.7)[b]		
23	283 (sh)[a]	321 (27)[a]	471 (7.8)[b]		
24	288 (14)[a]	356 (28)[a]	519 (10)[b]		

[a] Ligand-based process. [b] Phenolate to molybdenum LMCT process. [c] Molybdenum to pyridyl MLCT process. [d] Phenolate to methylpyridinium intra-ligand process. [e] Phenolate to tungsten LMCT process.

Electronic Spectroscopy. The electronic spectral data are summarized in Table IV; those bands which may be assigned with reasonable confidence are described in the footnotes. The variations in the spectra as the ligand changes in each set of four complexes are generally consistent with the relative ease of communication across the ligands that was established electrochemically. In particular, we have shown that electrochemical communication between the two ends of ligand L^3 is very weak in comparison to those in the isomeric ligands L^2 and L^4, by virtue of the substitution pattern of the aromatic rings, and the same behavior is apparent in the electronic spectra. For example, the phenolate to molybdenum LMCT transition of **3** (λ_{max} = 459 nm) is very similar to that of [MoL*(NO)Cl(OPh)] (λ_{max} = 464 nm); L^3 therefore behaves like an unsubstituted phenolate, with the negative charge trapped and unable to delocalize onto the pyridyl substituent. By contrast, for **1**, **2**, and **4** (λ_{max} = 486, 529, and 530 nm, respectively), the increasing conjugation of the ligand results in a progressive raising of the HOMO and a concomitant decrease in the LMCT energy as the negative charge is delocalized, with L^2 and L^4 giving nearly identical results. A similar pattern is evident for the ligand-based transition, which is at higher energy in **3** (λ_{max} = 305 nm) than it is for in **2** and **4** (λ_{max} = 323 and 322 nm, respectively). The pattern of absorptions in the tungsten complexes **13–16** is similar, with the energies of the LMCT and ligand-based transitions following the same order as they do for **1–4**.

In $[9]^+$, $[10]^+$, and $[12]^+$, the N-methylated analogues of **1**, **2**, and **4**, the phenolate-to-molybdenum LMCT bands are blue-shifted by 50–80 nm, appearing at 410, 470, and 480 nm respectively, due to a decrease in energy of the occupied ligand orbitals. By contrast, comparison of the spectra of **3** and $[11]^+$ show that the LMCT band has not moved; i.e., methylation of the pendant pyridyl group of L^3 has no measurable effect on the LMCT interaction involving the phenolate group, since the two fragments are electronically isolated. This is consistent with the electrochemical results which showed that N-methylation of **3** had virtually no effect on the redox potentials of the metal center. Likewise, the intense intraligand phenolate-to-methylpyridinium charge transfer (which will result in a quinonoidal contribution to the ligand structures as depicted in Figure 3) is at higher energy in $[11]^+$ than in $[10]^+$ or $[12]^+$, consistent with poor electronic communication between the ends of L^3. The same pattern of behavior repeats itself for the methylated tungsten complexes $[17]^+$–$[20]^+$.

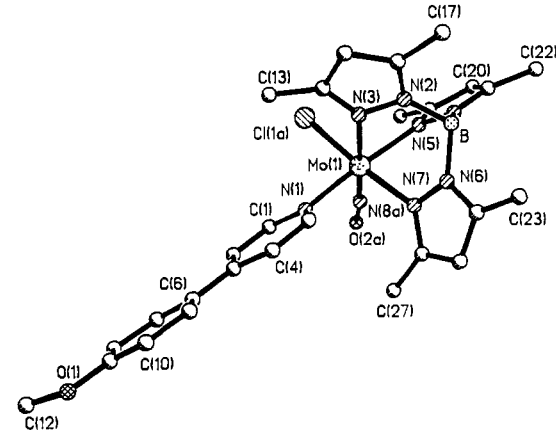

Figure 6. Molecular structure of [MoL*(NO)ClL^5] (**5**) showing the crystallographic numbering scheme.

The spectra of binuclear complexes **21–24** are, with minor pertubations, a composite of the spectra of the component parts; the weak MLCT transitions of the pyridyl–molybdenum center are hidden by the much more intense LMCT transitions of the phenolate–molybdenum center, but in the UV region peaks corresponding to both of the component parts are clearly visible.

Structural Studies. The presence of metal–metal and metal–methylpyridinium interactions across L^1 in these complexes suggests that the bridging ligand adopts a planar or near-planar conformation in solution due to a quinonoidal contribution to its structure. Although we have been unable to obtain good-quality crystals of any complexes containing L^1, support for this view comes from the crystal structure of **5**, which is shown in Figure 6. Selected bond lengths and angles are given in Table V, and atomic coordinates in Table VI. The coordination geometry is approximately octahedral. The most interesting feature of the structure is that the phenyl and pyridyl rings are nearly coplanar, with a dihedral angle of just 5° between them. This may interpreted in one of two ways. The ligand LUMO may be significantly occupied due to π-acidic character of the pyridine ligand. This is the explanation that was advanced to explain the near-planarity of a 4-phenylpyridine ligand bonded to titanium;[27] it was argued that the small dihedral angle (5°) was a consequence of the ligand formally being a radical anion, with near-planarity being the most efficient way to delocalize the high electron density. There is no evidence for superhyperfine coupling to hydrogen or nitrogen atoms in the EPR spectrum of **5**, but this is not surprising as the presence of five inequivalent nitrogen atoms in the coordination sphere of **5** would render any superhyperfine coupling too broad to observe. Although pyridyl ligands are generally considered to be good π-acceptors, the presence of the electron-donating methoxyphenyl substituent in **5** makes this explanation less likely.

The alternative explanation is exactly the converse and similar to the arguments already used to explain the behavior of L^1, i.e. that there is charge transfer from the electron-donating methoxy group to the pyridyl group, resulting in partial double-bond character between the two aromatic rings. The partial negative charge on the pyridyl N atom that this entails would be stabilized by coordination to a 17-electron metal center; the ligand is therefore acting as a π-donor, rather than as a π-acceptor. The fact that the 4-phenylpyridine (ppy) ligands in [Mo(NO)L*-(ppy)$_2$]$^+$ (which is isoelectronic with **5**) have inter-ring torsion

(27) Durfee, L. D.; Hill, J. E.; Kerschner, J. L.; Fanwick, P. E.; Rothwell, I. P. *Inorg. Chem.* **1989**, *28*, 3095.

Table V. Selected Internuclear Distances (Å) and Angles (deg) for [MoL*(NO)ClL^5] (**5**), with Estimated Standard Deviations in Parentheses

Mo(1)–N(1)	2.204(5)	Mo(1)–N(3)	2.246(5)	Mo(1)–N(5)	2.163(5)	Mo(1)–N(7)	2.196(5)
Mo(1)–Cl(1A)	2.432(6)	Mo(1)–N(8A)	1.846(21)	N(8A)–O(2A)	1.062(29)	N(1)–C(1)	1.335(10)
N(1)–C(5)	1.323(9)	C(1)–C(2)	1.362(10)	C(2)–C(3)	1.408(11)	C(3)–C(4)	1.389(10)
C(3)–C(6)	1.476(9)	C(4)–C(5)	1.377(9)	C(6)–C(7)	1.373(10)	C(6)–C(11)	1.390(11)
C(7)–C(8)	1.389(9)	C(8)–C(9)	1.380(11)	C(9)–C(10)	1.364(11)	C(9)–O(1)	1.370(8)
C(10)–C(11)	1.364(10)	O(1)–C(12)	1.406(10)				

Cl(1A)–Mo(1)–N(8A)	91.2(6)	Cl(1A)–Mo(1)–N(1)	93.6(2)	N(8A)–Mo(1)–N(1)	92.0(6)
Cl(1A)–Mo(1)–N(3)	89.7(2)	N(8A)–Mo(1)–N(3)	178.6(6)	N(1)–Mo(1)–N(3)	86.9(2)
Cl(1A)–Mo(1)–N(5)	95.4(2)	N(8A)–Mo(1)–N(5)	96.5(6)	N(1)–Mo(1)–N(5)	167.5(2)
N(3)–Mo(1)–N(5)	84.5(2)	Cl(1A)–Mo(1)–N(7)	174.3(2)	N(8A)–Mo(1)–N(7)	94.4(6)
N(1)–Mo(1)–N(7)	87.4(2)	N(3)–Mo(1)–N(7)	84.7(2)	N(5)–Mo(1)–N(7)	82.8(2)
Mo(1)–N(8A)–O(2A)	175.1(20)	Mo(1)–N(1)–C(1)	123.8(5)	Mo(1)–N(1)–C(5)	120.5(4)
C(1)–N(1)–C(5)	115.6(6)	N(1)–C(1)–C(2)	124.4(8)	C(1)–C(2)–C(3)	120.7(8)
C(2)–C(3)–C(4)	114.0(6)	C(2)–C(3)–C(6)	122.2(6)	C(4)–C(3)–C(6)	123.7(6)
C(3)–C(4)–C(5)	121.2(7)	N(1)–C(5)–C(4)	124.0(6)	C(3)–C(6)–C(7)	123.0(6)
C(3)–C(6)–C(11)	120.9(6)	C(7)–C(6)–C(11)	116.1(6)	C(6)–C(7)–C(8)	122.7(7)
C(7)–C(8)–C(9)	119.4(7)	C(8)–C(9)–C(10)	118.6(7)	C(8)–C(9)–O(1)	124.0(6)
C(10)–C(9)–O(1)	117.4(7)	C(9)–C(10)–C(11)	121.5(8)	C(6)–C(11)–C(10)	121.8(8)
C(9)–O(1)–C(12)	118.8(6)				

Table VI. Atomic Coordinates (×10^4) for **5**, with Estimated Standard Deviations in Parentheses

	x	*y*	*z*
Mo(1)	2255(1)	3864(1)	2356(1)
Cl(1A)	−55(5)	3696(4)	2331(3)
Cl(1B)	2520(17)	6057(9)	2263(11)
N(8A)	2407(18)	5554(20)	2263(12)
O(2A)	2421(17)	6525(18)	2232(11)
N(8B)	755(65)	3813(28)	2283(17)
O(2B)	−717(43)	3904(35)	2133(29)
N(1)	2064(5)	3375(5)	858(3)
C(1)	1345(8)	3902(8)	252(5)
C(2)	1210(9)	3599(8)	−674(5)
C(3)	1869(6)	2697(6)	−1062(4)
C(4)	2628(7)	2173(6)	−421(5)
C(5)	2697(7)	2530(6)	505(4)
C(6)	1735(6)	2336(6)	−2062(4)
C(7)	1051(7)	2922(6)	−2688(5)
C(8)	885(8)	2544(7)	−3626(5)
C(9)	1465(7)	1572(6)	−3956(5)
C(10)	2166(9)	995(7)	−3342(5)
C(11)	2312(8)	1369(7)	−2422(5)
O(1)	1362(5)	1127(5)	−4867(3)
C(12)	523(8)	1597(7)	−5508(5)
N(2)	2974(5)	1427(4)	3082(4)
N(3)	2098(5)	1803(5)	2440(4)
C(14)	1232(7)	789(6)	2070(5)
C(15)	1543(8)	−237(7)	2467(6)
C(16)	2649(8)	181(6)	3106(5)
C(17)	3389(10)	−523(7)	3747(7)
C(13)	119(8)	818(8)	1350(6)
N(4)	3604(5)	3376(5)	4217(3)
N(5)	2741(5)	4067(4)	3833(3)
C(21)	3807(7)	3682(6)	5137(4)
C(20)	3072(7)	4564(6)	5346(5)
C(19)	2411(7)	4803(6)	4532(4)
C(18)	1472(8)	5664(8)	4358(6)
C(22)	4702(8)	3110(7)	5772(5)
N(6)	4863(5)	3016(5)	2923(3)
N(7)	4323(5)	3829(5)	2419(3)
C(26)	5229(6)	4333(6)	1952(5)
C(25)	6330(7)	3825(7)	2142(5)
C(24)	6080(7)	2982(6)	2770(5)
C(27)	5004(8)	5291(8)	1341(6)
C(23)	6916(8)	2187(8)	3198(7)
B	4112(7)	2382(7)	3615(5)
C(28)	3375(21)	8559(13)	904(11)
Cl(2)	2977(10)	7951(8)	−111(4)
Cl(3)	4542(4)	9849(3)	1223(3)

angles of 30 and 41° [28] suggests that the latter explanation is correct. It is to be expected that double-bond character between the aromatic rings of L^5 would result in shortening of the bond,

(28) McQuillan, F.; Jones, C. J.; McCleverty, J. A.; Hamor, T. A. Unpublished results.

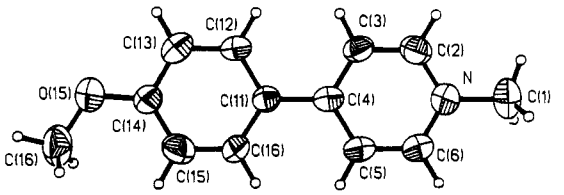

Figure 7. Molecular structure of the cation of [L^5-Me][PF$_6$] showing the crystallographic numbering scheme.

but the C–C distance of 1.476(9) Å in **5** is close to the average for biphenyl-type structures[29] and not significantly different from the analogous distances of 1.430(15) and 1.497(13) Å for the 4-phenylpyridine ligands in [Mo(NO)L*(ppy)$_2$]$^+$. The C=C distance between rings in a biphenylquinone-type structure is expected to be in the region of 1.35 Å.[30] It is possible that the degree of quinonoid character in L^5 is relatively small, as the MeO group is a less effective electron donor than O$^-$. The fact that the ligand is planar in the solid state does not guarantee that the same conformation occurs in solution but is consistent with the presence of electronic interactions across L^1 in [**9**]$^+$ and **21**. Although near-planarity of biphenyl-type groups is often a consequence of favorable stacking interactions between aromatic rings in the solid state,[29] this effect does not appear to be operating for **5** since the aromatic rings are not especially close to any other groups in the crystal.

If L^5 is behaving as a π-donor to a formally electron-deficient metal center, then from the point of view of the ligand, the analogy between coordination to a metal center and N-methylation is a reasonable one.[24] We accordingly determined the crystal structure of [L^5-Me][PF$_6$], which was prepared by methylation of L^5 with CH_3I followed by metathesis of the counterion with KPF_6, to determine its conformation. The structure of the cation is shown in Figure 7; bond lengths and angles are given in Table VII, and atomic coordinates, in Table VIII. The molecule is nearly planar with a torsion angle between the two rings of ca. 5°. However, in this case, there are obvious intermolecular π-stacking interactions in the lattice, with the methoxyphenyl ring of one molecule parallel to and overlapping with the N-methylpyridinium ring of an adjacent molecule; the mean inter-ring separation is ca. 3.4 Å, which is similar to the stacking distances observed in nucleic acids[31] and typical of the stacking distances observed in a wide variety of inorganic complexes containing aromatic ligands. The stacked rings are not eclipsed but slightly offset such that a

(29) Brock, C. P.; Minton, R. P. *J. Am. Chem. Soc.* **1989**, *111*, 4586.
(30) Allen, F. H.; Kennard, O.; Watson, D. G.; Brammer, L.; Orpen, A. G.; Taylor, R. *J. Chem. Soc., Perkin Trans. 2* **1987**, S1.
(31) Ts'O, P. O. P., Ed. *Basic Principles in Nucleic Acid Chemistry*; Academic Press: New York, 1974.

Table VII. Selected Internuclear Distances (Å) and Angles (deg) for [L^5-Me][PF_6], with Estimated Standard Deviations in Parentheses

C(1)–N	1.463(15)	N–C(2)	1.340(13)	N–C(6)	1.328(15)	C(2)–C(3)	1.361(16)
C(3)–C(4)	1.386(14)	C(4)–C(5)	1.383(12)	C(4)–C(11)	1.476(14)	C(5)–C(6)	1.381(16)
C(11)–C(12)	1.378(12)	C(11)–C(16)	1.384(13)	C(12)–C(13)	1.397(15)	C(13)–C(14)	1.385(15)
C(15)–C(16)	1.373(17)	C(15)–C(14)	1.364(14)	O(15)–C(16)	1.436(15)	O(15)–C(14)	1.355(13)
P–F(1)	1.543(9)	P–F(2)	1.495(11)	P–F(3)	1.541(10)	P–F(4)	1.494(11)
P–F(5)	1.381(19)	P–F(6)	1.488(18)				

C(1)–N–C(2)	120.9(9)	C(1)–N–C(6)	120.4(8)	C(2)–N–C(6)	118.7(9)
N–C(2)–C(3)	122.7(10)	C(2)–C(3)–C(4)	119.9(8)	C(3)–C(4)–C(5)	116.7(9)
C(3)–C(4)–C(11)	121.4(8)	C(5)–C(4)–C(11)	121.9(9)	C(4)–C(5)–C(6)	120.8(9)
N–C(6)–C(5)	121.2(9)	C(4)–C(11)–C(12)	121.4(8)	C(4)–C(11)–C(16)	121.4(8)
C(12)–C(11)–C(16)	117.2(9)	C(11)–C(12)–C(13)	121.6(9)	C(12)–C(13)–C(14)	119.4(9)
C(16)–C(15)–C(14)	120.7(10)	C(11)–C(16)–C(15)	121.8(8)	C(16)–O(15)–C(14)	118.1(8)
C(13)–C(14)–C(15)	119.3(10)	C(13)–C(14)–O(15)	114.8(8)	C(15)–C(14)–O(15)	125.9(10)

Table VIII. Atomic Coordinates ($\times 10^4$) for [L^5-Me][PF_6], with Estimated Standard Deviations in Parentheses

	x	*y*	*z*
P	1919(5)	8400(1)	9084(3)
F(1)	−246(14)	8162(5)	8332(8)
F(2)	1870(20)	8765(6)	7876(9)
F(3)	4160(15)	8600(5)	9785(9)
F(4)	2013(18)	7996(6)	10231(9)
F(5)	1151(29)	8853(8)	9714(17)
F(6)	2830(24)	7920(8)	8432(14)
C(1)	7790(18)	12292(5)	4949(12)
N	6158(13)	11922(4)	5278(9)
C(2)	4603(18)	11703(5)	4316(10)
C(3)	3045(15)	11362(5)	4581(9)
C(4)	2972(15)	11251(4)	5892(9)
C(5)	4593(17)	11477(4)	6874(9)
C(6)	6162(17)	11809(5)	6544(11)
C(11)	1256(14)	10903(4)	6217(8)
C(12)	−508(16)	10752(4)	5251(9)
C(13)	−2155(16)	10432(4)	5558(10)
C(15)	−254(19)	10397(5)	7820(11)
C(16)	1329(15)	10724(5)	7511(10)
O(15)	−3689(11)	9951(3)	7056(7)
C(16)	−3662(19)	9757(5)	8386(12)
C(14)	−2007(16)	10256(4)	6862(10)

hydrogen atom of one ring is above the center of the other, which has been shown to be the optimal orientation for face-to-face π-stacking.[32] Although the electronic spectra confirm that the intra-ligand charge transfer is at lower energy in [L^5-Me][PF_6] than in L^5 (λ_{max} = 353 and 276 nm; ϵ = 7000 and 21 000 M^{-1} cm^{-1} respectively), it is not possible in this case to determine whether the planar conformation is due to these electronic effects or to crystal-packing effects; also the relatively poor quality of the data means that detailed discussion of bond lengths and angles is probably inappropriate. The near-planarity is in contrast to the analogous methylated acridine bearing a 4-methoxyphenyl substituent, which has a torsion angle of 88° between the phenyl and acridine sections in the solid state,[33] but this may be a steric effect due to interaction of the acridine H^1 and H^8 protons with H^2 and H^6 of the phenyl ring.

Conclusion. We have prepared a series of mono- and binuclear complexes with a new series of asymmetric bridging ligands bearing a pyridyl donor at one end and a phenol at the other. The electrochemical interactions across these bridging ligands indicate (i) that L^1, which is in principle capable of free rotation about the interannular bond, adopts a near-planar conformation due to partial quinonoid structure arising from charge transfer between the electron-donating phenolate group and the electron-accepting pyridyl group and (ii) that the magnitude of the electrochemical interaction is related to both the inter-metal separation (comparison of L^1 with L^2) and the extent to which the bridging ligand can form a delocalized, quinonoid structure (comparison of L^2, L^3, and L^4). These results are of relevance to controlling electronic interactions along "molecular wires". The EPR spectra of the 34-electron (17 + 17) biradicals indicate that, despite a difference of about 0.8 V in the redox potentials of the metal centers at each end of the bridging ligand, the two unpaired electrons undergo fast exchange on the EPR time scale. These are the first examples of fast exchange in asymmetric biradical, bimetallic complexes.

Acknowledgment. We wish to thank to the SERC for a postdoctoral fellowship (to A.D.) and for the funds to purchase the EPR spectrometer.

Supplementary Material Available: Tables of atomic coordinates and equivalent isotropic displacement coefficients, bond lengths, bond angles, and anisotropic displacement coefficients (5 pages). Ordering information is given on any current masthead page.

(32) (a) Jorgensen, W. L.; Severance, D. L. *J. Am. Chem. Soc.* **1990**, *112*, 4768. (b) Hunter, C. A.; Sanders, J. K. M. *J. Am. Chem. Soc.* **1990**, *112*, 5525.

(33) Goubitz, K.; Reiss, C. A.; Heijdenrijk, D. *Acta Crystallogr., Sect. C* **1990**, *46*, 1081. Janker, S. A.; Ariese, F.; Verhoeven, J. W. *Recl. Trav. Chim. Pays-Bas* **1989**, *108*, 109.